UCLA
COMPUTATIONAL AND APPLIED MATHEMATICS

Progress in Boundary Layer Control: Robust Reduced-Order Control of Skin-Friction Drag

L. Cortelezzi
K.H. Lee
J. Kim
J.L. Speyer

March 1998

CAM Report 98-14

Department of Mathematics
University of California, Los Angeles
Los Angeles, CA. 90024-1555

Progress in Boundary Layer Control: Robust Reduced-Order Control of Skin-Friction Drag

by L. CORTELEZZI, *,1,2 K.H. LEE,[1] J. KIM,[1] and J.L. SPEYER[1]

[1] Department of Mechanical and Aerospace Engineering
University of California, Los Angeles, California 90095-1597
[2] Department of Mathematics
University of California, Los Angeles, California 90095-1555

March 25, 1998

Abstract

A successful application of a linear controller to a two-dimensional channel flow is presented. An optimal and robust reduced-order linear feedback controller is derived by using multi-variable linear-quadratic-Gaussian synthesis, or, in modern term, $\mathcal{H}_2$ synthesis, combined with model reduction techniques. This controller based on a reduced-model of the linearized Navier-Stokes equations is applied to suppress finite-amplitude near-wall disturbances in a channel flow at Re=1500. The controller efficiently reduced near-wall disturbances obtaining a substantial drag reduction and eventually the flow is relaminarized.

*Corresponding author: Telephone (310) 206-2732, Facsimile (310) 206-6673, E-mail: crtlz@math.ucla.edu

1 Introduction

Wide attention has been given to the problem of reducing wall-shear stresses generated by near-wall turbulence, or, in other words, to the problem of reducing drag produced by skin friction. "The skin friction constitutes about 50%, 90%, and 100% of the total drag on commercial aircraft, underwater vehicles, and pipelines, respectively" [1]. Consequently, important economic and environmental benefits will spring from the successful and reliable control of near-wall turbulence.

In the recent years, boundary layer control has been attempted by several investigators with some success [5]-[24]. However, controllers able to analyze distributed measurements and coordinate distributed actuators are regarded by the fluid mechanics community as essential for achieving better results. Tools for designing this class of controllers have been developed by the control community over the past two decades [25]-[26]. Very little has been done to exploit these tools in connection with the control of boundary layers [27]-[29] because of the belief that linear controllers are not suited for controlling a nonlinear phenomenon, like wall turbulence.

Recently, Cortelezzi and Speyer [30] used multi-input-multi-output (MIMO) linear quadratic Gaussian (LQG) synthesis, or, in modern terms, $\mathcal{H}_2$ synthesis, combined with model reduction techniques for designing an optimal and robust linear feedback controller able to suppress wall-disturbances leading to transitions in a two-dimensional laminar channel flow. The present paper shows that the controller derived by Cortelezzi and Speyer, based on a reduced-model of the linearized Navier-Stokes equations, can be successfully applied to the control of skin-friction drag in a two-dimensional channel flow. This is an essential intermediate step toward the derivation and application of this class of controllers to three-dimensional boundary layers.

The intermediate step of controlling skin-friction drag in a two-dimensional channel flow will perhaps disappoint some readers because of the fundamental differences between two and three-dimensional turbulent channel flows. Turbulence is essentially a three-dimensional phenomenon. Consequently, results obtained by controlling skin-friction drag in two-dimension cannot be readily extrapolated to the three-dimensional case. However, the derivation and testing of optimal and robust reduced-order linear feedback controller in a two-dimensional environment has been very valuable for understanding the potentiality of MIMO LQG, $\mathcal{H}_2$, synthesis and model reduction in relation to boundary layer control problem.

In Section 2, we formulate the problem in terms of Navier-Stokes equations and we provide details about the numerical scheme used to integrate them. In Section 3, we derive the state space equations from the linearized Navier-Stokes equations. In Section 4, we reduce the order of the state space equations and derive an optimal and robust reduce-order controller by using LQG, $\mathcal{H}_2$ synthesis. In Section 5 we apply the controller to a turbulent channel flow at Re=1500 and discuss its performance. Conclusions will close the article.

2 Mathematical Formulation

We consider the turbulent flow of an incompressible fluid in a two-dimensional periodic channel of length Lh and height $2h$, see Figure 1. This problem is governed by the Navier-Stokes and continuity

equations

$$\frac{\partial u}{\partial t} + u\frac{\partial u}{\partial x} + v\frac{\partial u}{\partial y} = -\frac{\partial p}{\partial x} + \frac{1}{Re}\triangle u, \qquad (1)$$
$$\frac{\partial v}{\partial t} + u\frac{\partial v}{\partial x} + v\frac{\partial v}{\partial y} = -\frac{\partial p}{\partial y} + \frac{1}{Re}\triangle v,$$

$$\frac{\partial u}{\partial x} + \frac{\partial v}{\partial y} = 0 \qquad (2)$$

where $\triangle$ is the two-dimensional Laplacian. We made the problem dimensionless by using h as characteristic length and h/U_c as characteristic time, where U_c is the velocity at the center of the channel. The Reynolds number is $Re = U_c h/\nu$.

We apply blowing and suction at the bottom wall to suppress near-wall turbulence within the bottom boundary layer. To simplify the problem the actuators are assumed uniformly distributed along the bottom wall. Near-wall turbulence within the top boundary layer is left free to evolve. The corresponding boundary conditions are

$$u(x, \pm 1, t) = v(x, 1, t) = 0, \qquad v(x, -1, t) = v_w(x, t). \qquad (3)$$

The control function v_w prescribes the amount of blowing and suction at the wall. In the next Section, we will impose that the amount of fluid removed equals the amount of fluid injected.

We measure the gradient of the streamwise velocity at given points $x = x_i$ to detect and measure near-wall turbulence within the bottom boundary layer. In other words, we measure the first term of the wall-shear stresses, $\tau_{yx} = Re^{-1}(\partial u/\partial y + \partial v/\partial x)|_{y=-1}$, i.e.

$$z(x_i, t) = \left.\frac{\partial u}{\partial y}\right|_{x=x_i, y=-1}. \qquad (4)$$

Note that the second term of the wall-shear stresses is known when the actuators operate while is zero in the uncontrolled case.

Time dependent incompressible Navier-Stokes equations (1)-(3) with the appropriate initial condition are integrated numerically using a semi-implicit fractional step method. The second order-implicit Crank-Nicolson is used for the viscous terms and the nonlinear convective terms are advanced using a 3^{rd}-order low-storage Runge-Kutta scheme.

A staggered grid is used in the computation. All spatial derivatives are discretized with a 4^{th}-order compact finite-difference scheme. A uniform grid is used in the streamwise direction, while a nonuniform grid corresponding to Chebyshev collocation points is used in the wall-normal direction. We simulate turbulent channel flows on a computational domain of $4\pi \times 2$ with a resolution of 512×64. Detailed descriptions of the numerical methods used to simulate the flow under investigation are given in Ref. [31].

3 Derivation of the State-Space Equations

In this section we outline the derivation of the state-space equations [30]. To derive the state-space equations we first linearize equations (1) with respect to the laminar velocity field $U(y) = U_c(y^2 - h^2)$, see Figure 1. The linearized Navier-Stokes equations are written in terms of the stream-function ψ to identically satisfy continuity,

$$(\frac{\partial}{\partial t} + U\frac{\partial}{\partial x})\triangle\psi - \frac{d^2U}{dy^2}\frac{\partial\psi}{\partial x} = \frac{1}{Re}\triangle\triangle\psi, \qquad (5)$$

and corresponding boundary conditions are

$$\left.\frac{\partial\psi}{\partial x}\right|_{y=-1} = -v_w(x,t), \qquad \left.\frac{\partial\psi}{\partial y}\right|_{y=\pm1} = \psi(x,1,t) = 0. \tag{6}$$

The measurement equation (4) becomes

$$z(x_i,t) = \left.\frac{\partial^2\psi}{\partial y^2}\right|_{y=-1}. \tag{7}$$

The design of a controller for the LQG ($\mathcal{H}_2$) problem is contingent on the definition of an optimal performance index, or cost function. A cost function should be constructed with the intent of simultaneously minimizing near-wall turbulence and the cost of the controller. It is crucial to minimize the cost of the controller because the energy available to drive the controller is limited in any engineering application. Furthermore, the system could be driven away from the region where the linear model is valid by large control action. Because of the high correlation between near-wall turbulence and wall-shear stresses, we choose the following cost function:

$$J = \lim_{t_f\to\infty}\int_t^{t_f}\int_0^L \left[\left(\frac{\partial^2\psi}{\partial y^2}\right)^2 + \left(\frac{\partial^2\psi}{\partial x^2}\right)^2\right]_{y=-1} dx\,dt. \tag{8}$$

The integrand represents the cost of the wall-shear stresses being different from zero. Moreover, the second term of the integrand implicitly accounts for the cost of implementing the control itself.

To reduce (5)-(7) to a set of first-order ordinary differential equations, we make a few transformations as shown in Ref. [30]. Taking advantage of the linearity of the problem, we assume that the stream-function ψ is the sum by two parts: a modified stream-function ϕ which satisfies to the equation (5) with homogeneous boundary condition, and a function χ which satisfies to the non-homogeneous boundary conditions forming a forcing function to (5). Subsequently, flow quantities are spectrally decomposed by using circular functions in the streamwise direction and Chebyshev polynomials in the vertical direction. We expand ϕ and χ as follows:

$$\phi(x,y,t) = \sum_{n=1}^{N}\sum_{m=0}^{M}[a_{nm}(t)\cos(\alpha_n x) + b_{nm}(t)\sin(\alpha_n x)]C_m(y), \tag{9}$$

$$\chi(x,y,t) = \sum_{n=1}^{N}[p_n(t)\cos(\alpha_n x) + q_n(t)\sin(\alpha_n x)]D(y). \tag{10}$$

where $\alpha_n = 2\pi n/L$. Functions C_m and D are combinations of Chebyshev polynomials constructed to satisfy the boundary conditions, i.e.,

$$C_m(y=\pm1) = \left.\frac{dC_m}{dy}\right|_{y=\pm1} = 0, \qquad D(y=-1) = 1, \qquad D(y=1) = \left.\frac{dD}{dy}\right|_{y=\pm1} = 0. \tag{11}$$

We also expand the measurement function z as follows:

$$z(x,t) = \sum_{n=1}^{N}[c_n(t)\cos(\alpha_n x) + d_n(t)\sin(\alpha_n x)]. \tag{12}$$

We substitute expansions (9), (10), and (12) into the evolution and measurement equations (5)-(7) and use Galerkin's projection to obtain a set of ordinary differential equations. These equations are cast by matrix transformations into the following state-space equations:

$$\frac{d\boldsymbol{x}}{dt} = \boldsymbol{A}\,\boldsymbol{x} + \boldsymbol{B}\,\boldsymbol{u}\,, \qquad \boldsymbol{z} = \boldsymbol{C}\,\boldsymbol{x} + \boldsymbol{D}\,\boldsymbol{u}\,, \tag{13}$$

with initial condition $\boldsymbol{x}\ (0) = \boldsymbol{x_0}$. The vectors $\boldsymbol{x}$, $\boldsymbol{u}$, and $\boldsymbol{z}$ are the internal state vector, the control vector, and the measurement vector, respectively. The dynamics of the Poiseuille flow, actuators and sensors, are contained into the matrices $\boldsymbol{A}$, $\boldsymbol{B}$, and $\boldsymbol{C}$, respectively, while the direct coupling between sensors and actuators is contained into the matrix $\boldsymbol{D}$. Note that this coupling would be eliminated if actuators dynamics could be explicitly imposed. The cost function (8) becomes

$$J = \lim_{t_f \to \infty} \int_t^{t_f} [\boldsymbol{z}^T \boldsymbol{z} + \boldsymbol{u}^T \boldsymbol{W}^T \boldsymbol{W}\ \boldsymbol{u}\ ] dt, \tag{14}$$

where the superscript ^{T} denotes transpose. The matrix $\boldsymbol{W}$ is generated by spectral decomposition of the last term in the cost function (8).

The main advantage of this formulation is the decoupling of the problem with respect to the wave number where all matrices in (13) and (14) are block diagonal. Consequently, the state-space system (13) is equivalent to N state-space sub-systems, one for each wave number. The state-space equations for a given wave number r are

$$\frac{d\boldsymbol{x_r}}{dt} = \boldsymbol{A_r}\ \boldsymbol{x_r} + \boldsymbol{B_r}\ \boldsymbol{u_r}\ , \qquad \boldsymbol{z_r} = \boldsymbol{C_r}\ \boldsymbol{x_r} + \boldsymbol{D_r}\ \boldsymbol{u_r}\ , \tag{15}$$

with initial condition $\boldsymbol{x_r}\ (0) = \boldsymbol{x_{r0}}$. The structure of vectors $\boldsymbol{x_r}$, $\boldsymbol{u_r}$, $\boldsymbol{z_r}$ is the following: $\boldsymbol{x_r} = [a_{r0}, \cdots a_{rM}, b_{r0}, \cdots b_{rM}]^T$, $\boldsymbol{u_r} = [p_r, q_r]^T$, $\boldsymbol{z_r} = [c_r, d_r]^T$. The cost function (14) also decouples with respect to the wave number. It is the sum of N optimal performance indexes J_r. The cost function for a given wave number r is defined as follows

$$J_r = \lim_{t_f \to \infty} \int_t^{t_f} [\boldsymbol{z_r}^T \boldsymbol{z_r} + \boldsymbol{u_r}^T \boldsymbol{W_r}^T \boldsymbol{W_r}\ \boldsymbol{u_r}\ ] dt. \tag{16}$$

Consequently, the design of an optimal and robust controller for the system (13) with (14) has been reduced to the independent design of N optimal and robust controllers, one for each wave number, for the sub-systems (15) with (16).

4 Model Reduction and Controller Design

The size of the controller is a crucial parameter in any engineering applications because of the amount of hardware and computer power necessary to compute a real-time control law. Since a controller based on the full system would have $2N(M+1)$ states, where N=32 and M=64 is considered a simple case in literature, it is crucial to reduce the order of the controller. A low-order controller for the present problem can be derived in two steps [30]: First by constructing a lower order model of (15), and subsequently, by designing an optimal and robust controller for the reduced-order model.

In order to obtain a lower order model for each wave number, we transform each state-space subsystem (15) into Jordan Canonical form. This transformation decouples the modes of each subsystem, in other word it reduces the subsystem matrices to a block diagonal form. From the transformed $\boldsymbol{B_r}$ and $\boldsymbol{C_r}$ matrices the states that are equally well controllable and observable are determined. The matrices $\hat{\boldsymbol{A}}_r$, $\hat{\boldsymbol{B}}_r$, $\hat{\boldsymbol{C}}_r$, $\boldsymbol{D_r}$ that describe the dynamics of the reduced-order internal state-space subsystem are obtained from the matrices in Jordan Canonical form by removing rows and columns corresponding to poorly controllable or observable states. Hat denotes the quantities associated with the reduced-order model.

Although a rigorous mathematical framework for the design of disturbance attenuation ($\mathcal{H}_\infty$) linear controllers is provided by the control synthesis theory in [25]-[26], for this initial study LQG ($\mathcal{H}_2$) synthesis is quite adequate. In general, the the design of an optimal and robust linear feedback controller for the LQG ($\mathcal{H}_2$) problem is divided in two parts: linear-quadratic-regulator (LQR) and minimum variance estimator (Kalman-Bucy filter). The LQR design provides an optimal control law in terms of the internal state vector by minimizing a cost function. The internal state vector is essential to implement the control law but, in general, it is not a physical quantity directly measurable, but reconstructed from the measurement vector $\boldsymbol{z_r}$ by the estimator. Since we have assumed no statistics, the power spectral densities required for the minimum variance estimator are chosen as design parameters in order to keep the eigenvalues of the estimator at the same order of magnitude as the eigenvalues of the controller. In particular, the power spectral density of the process noise is chosen so that the resulting loop transfer matrix approximates the loop transfer matrix of the LQR which has significant robustness properties [32]-[33]. In this study the LQG ($\mathcal{H}_2$) design of an optimal and robust controller for each reduced-order state space subsystem (15) can be carried out in parallel. The final result of the LQG ($\mathcal{H}_2$) is summarized by the following equations:

$$\boldsymbol{u_r} = -\hat{\boldsymbol{K}}_r \, \tilde{\boldsymbol{x}}_r \, , \tag{17}$$

$$\frac{d\tilde{\boldsymbol{x}}_r}{dt} = \hat{\boldsymbol{A}}_r \, \tilde{\boldsymbol{x}}_r + \hat{\boldsymbol{B}}_r \, \boldsymbol{u_r} + \hat{\boldsymbol{L}}_r \, [\boldsymbol{z_r} - \hat{\boldsymbol{C}}_r \, \tilde{\boldsymbol{x}}_r - \boldsymbol{D_r} \, \boldsymbol{u_r}], \tag{18}$$

with initial conditions $\tilde{\boldsymbol{x}}_r \, (0) = \boldsymbol{0}$. Equation (17) is the control law. It predicts the optimal blowing and suction at the bottom wall by processing the estimated reduced-order internal state vector with the gains matrix $\hat{\boldsymbol{K}}_r$. The gains matrix $\hat{\boldsymbol{K}}_r$ is obtained by minimizing the following optimal performance index:

$$\hat{J}_r = \lim_{t_f \to \infty} \int_t^{t_f} [\hat{\boldsymbol{z}}_r{}^T \hat{\boldsymbol{z}}_r + \boldsymbol{u_r}{}^T \boldsymbol{W_r}{}^T \boldsymbol{W_r} \, \boldsymbol{u_r}] dt, \tag{19}$$

where $\hat{\boldsymbol{z}}_r = \hat{\boldsymbol{C}}_r \, \hat{\boldsymbol{x}}_r - \boldsymbol{D_r} \, \boldsymbol{u_r}$. Although equation (18) is the the minimum variance estimator in a statistical sense, this filter is essentially an observer that reconstructs from the measurements an estimate of the reduced-order internal state vector. However, when the estimator is eventually implemented in a system where the measurements and process dynamics are corrupted by noise, the Gaussian white noise assumption will be used to develop the filter gains. The initial condition $\tilde{\boldsymbol{x}}_r \, (0) = \boldsymbol{0}$ implies that the estimator starts with no information about $\hat{\boldsymbol{x}}_r$.

Note that the numerical integration of the estimator (18), the computation of the control law (17), and fast direct and inverse Fourier transforms can be programmed in a computer routine suited for parallel computing. Subsequently, this routine can be embedded in any Navier-Stokes solver for the control of simulated turbulent channel flows as shown in the next Section.

5 Results

We designed a controller for two-dimensional Poiseuille flow in a periodic channel of length $L = 4\pi$ at $Re = 1500$. We used a grid resolution of $N = 32$ and $M = 60$, consequently, the order of the full system is 3904. Using the model reduction technique previously described, we created 32 reduced models and derived 32 controllers of order 12, one for each state space subsystem (15). Controllers operate in parallel. The combined order of the controllers for all 32 wave numbers is 384, it represents a dramatic reduction, about 90%, with respect to the order of the full system.

This controller is tested on a two-dimensional turbulent channel flow at Re=1500. Since there are no unstable modes at Re=1500, we use a combination of channel and wall modes to create a worse scenario initial perturbation velocity field [34]. The maximum rms value of the initial perturbation velocity field is $u_{rms} = 0.3$, i.e. 30% of the centerline velocity of the undisturbed laminar flow. We construct the initial velocity field by superimposing a perturbation velocity field onto the laminar flow. The corresponding initial vorticity field produces pockets of positive and negative vorticity distributed along the center and walls of the channel. Although the initial disturbances in the two-dimensional channel flow will eventually decay, they permit testing the capability of the controller in suppressing near-wall turbulence that can increase drag and trigger boundary layer eruptions and flow separations in turbulent boundary layers. Note that this initial condition includes nonlinear effects that are not included in the linear model and also stimulates modes that are not included in the reduced-order model, and consequently, cannot be directly controlled.

Figure 2 presents a comparison of the vorticity field in the controlled and uncontrolled cases at time t=2 and 4. Figure 2 also presents the amplitude of blowing and suction applied to the bottom wall of the channel. In the uncontrolled case, at time t=2, two large pockets of negative and positive vorticity can be recognized on the left along the bottom wall, while minor vortical structures populate the remaining part of the boundary layer. At time t=4, the interaction of the two pockets of vorticity with the rest of the flow generates an eruption of fluid toward the center of the channel. A large negative vortex entrains some of the positive vorticity from the wall increasing the separation. A similar process takes place on a smaller scale further downstream. Flow separation also occurs at the top boundary layer; a large eruption can be recognized on the left and two smaller eruptions further downstream.

In the controlled case, at time t=2, the vorticity field near the bottom wall is strongly modified by the action of the controller, see Figure 2. Pockets of high positive vorticity have been removed while pockets of high negative vorticity have been lifted away from the wall. Only low negative vorticity can be recognized within the bottom boundary layer. The plot of v_w shows that the controller tends to inject fluid underneath pockets of negative vorticity while it tends to remove fluids in correspondence with pockets of positive vorticity. At time t=4, the action of the controller can be more easily interpreted. The controller breaks the pockets of negative vorticity that have been lifted up into smaller vortical structure. These structures are made rolling along the bottom wall by injecting and removing fluid from the rear and the front of the vortical structure, respectively. Note that at time t=2 the controller affects only the flow near to the bottom wall leaving most of the vorticity field unaffected. At time t=4, however, the controller action has penetrated further toward the center of the channel because of the viscous and nonlinear effects.

Figure 3 presents a comparison of the vorticity field in the controlled and uncontrolled cases at time t=12 and 14. Figure 3 also presents the amplitude of blowing and suction applied to the bottom wall of the channel. The uncontrolled case shows the evolution of a major eruption along the bottom wall that affects nearly half of the bottom boundary layer as well as part of the top boundary layer. In particular, the pairing process of two large negative vortical structures interacts with a pocket of positive vorticity on the bottom wall. The vortex pairing entrains parts of the positive vorticity enhancing the separation of the flow. In the controlled case almost the entire vorticity field has been strongly modified by the controller, high values of vorticity are confined to the top boundary layer. Near to the bottom wall three negative vortical structures are kept rolling by the controller action although there is no significant vorticity along the wall. As in the previous figure, the controller injects and removes fluid from the rear and the front of the vortical structures, respectively. In this figure is easy to see that v_w changes sign at the streamwise locations corresponding with the center of the vortical structures. The action of the controller has also reduced the interaction between top and bottom boundary layers resulting in an mild attenuation of the near-wall turbulence at the top wall.

Figure 4 presents a comparison of the vorticity field in the controlled and uncontrolled cases at time t=50. Figure 4 also presents the amplitude of blowing and suction applied to the bottom wall of the channel. The uncontrolled case is dominated by the least stable modes, while all the other modes have been subdued by viscosity. Although the flow is slowly relaxing toward the laminar regime, the top and bottom boundary layers are still showing sign of flow separation. In the controlled case the flow has been nearly relaminarized over the entire computational domain. Correspondingly, blowing and suction at the bottom wall is nearly zero.

Figures 5 shows the spatial and temporal evolution of the wall-shear stresses in the uncontrolled case. The wall-shear stresses present a rich structure because of the near-wall turbulence generated by the initial condition. However, viscous effects eventually reduce the amplitude of the wall-shear stresses over time; turbulence in fact cannot sustain itself in a two-dimension channel flow at Re=1500.

Figure 6 presents the spatial and temporal evolution of the wall-shear stresses and blowing and suction in the controlled case. The controllers reduce the initial wall-shear stresses in the first few time steps although the estimators (18) start with no information about the reduced-order internal state vector. Subsequently, the amplitude of blowing and suction rises to suppress the effects of near-wall turbulence. Eventually, blowing and suction decreases as the near-wall turbulence subdues. Controlled wall-shear stresses show some waviness due to poorly controllable low wave number modes and some ripples at wave numbers higher than 32. Ripples quickly disappears after few time units, while low wave numbers waviness persists for longer time. By the end of the computation, $t = 50$, all the perturbations of the wall-shear stresses have been suppressed and the flow has been nearly relaminarized, see Figure 4. The wall-shear stresses have a nearly constant value 1.62. This value indicates that the average velocity profile near the bottom wall generates about 20% less drag than the parabolic profile. However, this more efficient profile will eventually relax to the parabolic profile due to the viscous effects.

Figures 2-6 indicates the successful performance of the 32 robust reduced-order linear controllers operating in parallel. It is not clear that it is necessary to control disturbances for all 32 wave numbers since disturbances correspondingly to high wave numbers are very quickly damped. Consequently there is hope for further reducing the size of the controller. Any further reduction of the size of the controller increases the potential of using the controller in engineering applications. To investigate this issue we ran the same simulation presented in Figures 2-6 with only 16 robust reduced-order controllers operating in parallel. The combined order of the controllers for 16 wave numbers is 192, a substantial reduction, 50%, with respect to the previous reduced-order controller, and about 95%, with respect to the order of the full system.

Figure 7 presents the spatial and temporal evolution of the wall-shear stresses in the controlled case when only the controllers corresponding to the 16 lowest wave numbers are operating. During the few time steps, when the turbulence structures span over all the wave numbers, this partially controlled case presents some noticeable differences with respect to the fully controlled case (Figure 6). The controller compensates for its inability of controlling high wave numbers by increasing the amplitude of blowing and suction at low wave numbers. Consequently, wall-shear stresses show some spikes corresponding to high wave number near-wall turbulence. However, beside these events the wall-shear stresses retain the same trend as in the fully controlled case. At later times, $t > 10$, the wall-shear stresses and blowing and suction at the wall present a trend very similar to the fully controlled case. The wall-shear stresses show some low amplitude waviness at wave numbers higher than 16. Blowing and suction at the wall present a slightly higher amplitude and deformation with respect to the fully controlled case. Nevertheless, the overall effect of the 16 wave numbers controller is a dramatic reduction of the wall-shear stresses and a almost complete relaminarization of the entire flow.

Drag reduction is the dominant reason driving the effort of controlling near-wall turbulence. To estimate the performance of the controller, we compute the drag by integrating the wall-shear stresses

along the bottom wall of the channel. Figure 8 compares the drag in the uncontrolled, laminar, fully controlled and partially controlled cases. The drag for the laminar case is exact and equals 2. In the uncontrolled and controlled cases the drag is initially 2 because the initial velocity field has been constructed by superimposing a zero-mean perturbation velocity field onto the laminar flow. In the uncontrolled case, the drag drops below the laminar value during the transient period followed by drag increases above the laminar value 2.46 and with some fluctuation reaches its maximum value around t=25. In the last half of the simulation the drag decreases toward the laminar value because turbulence is subdued by viscosity, since turbulence cannot sustain itself in a two-dimensional channel flow at this Reynolds number. In the fully controlled case, the drag presents some large fluctuation below the laminar value during the first few time units at the onset of the turbulent flow. The amplitude of the fluctuations reduces with time while the value of the drag stays at about half of the laminar value. In the later part of the simulation the controller affects the entire computational domain and the flow is nearly relaminarized. The drag in the partially controlled case is remarkably similar to the fully controlled case. This results substantiates the notion that it is not necessary to control all the wave numbers.

6 Conclusions

In this article we presented a successful application of robust reduced-order linear feedback control to a two-dimensional channel flow whose initial condition consist of finite-amplitude disturbances. A controller based on a reduced-model of the linearized Navier-Stokes equations, i.e. 10% of the order of the full size system, was designed by using LQG ($\mathcal{H}_2$) synthesis. This controller was programmed in a computer routine whose input measurements are the gradients of the streamwise velocity component and whose output controls are the blowing and suction at the wall. This routine, suited for parallel computing, was embedded in a direct numerical simulation of the Navier-Stokes equations. As a case study, we applied the controller to the bottom wall of a two-dimensional turbulent periodic channel flow at $Re = 1500$. The controller drastically reduced near-wall turbulence preventing boundary layer eruptions and flow separations and eventually relaminarized almost the entire flow. A dramatic drag reduction was obtained, up to 50% with respect to the laminar flow and up to 60% with respect to the turbulent flow. Extensions of LQG ($\mathcal{H}_2$) design and applications of $\mathcal{H}_\infty$ design [25]-[26] to three-dimensional channel flows and three-dimensional Blasius boundary layers are in progress.

7 Acknowledgment

The authors thank Dr. J. Burns, Dr. S. Joshi, Dr. R.E. Kelly, and Dr. R.T. MCloskey for the enlighting discussions. This work is supported by AFOSR Grant F49620-97-1-0276 and by NASA Grant NCC 2-374 Pr 41.

References

[1] M. Gad-el-Hak, (1994), Interactive control of turbulent boundary layers – A futuristic overview, *AIAA Journal*, **32**, (9), 1753.

[2] V.J. Modi, (1997), Moving surface boundary-layer control: A review. Journal of Fluids and Structures, **11**, (6),627-663.

[3] H.L. Reed, W.S. Saric and D. Arnal, (1996), Linear stability theory applied to boundary layers, Annu. Rev. Fluid Mech., **28**, 389.

[4] R.W. Barnwell and M.Y. Hussaini, (1992), *"Natural laminar flow and laminar flow control,"* (Springer-Verlag, New York).

[5] P. Koumoutsakos, (1997), Active control of vortex-wall interactions. Physics of Fluids, **9**, (12), 3808-3816.

[6] R. Rathnasingham and K.S. Breuer, (1997), System identification and control of a turbulent boundary layer. Physics of Fluids, **9**, (7), 1867-1869.

[7] C. Lee, J. Kim, D. Babcock, and R. Goodman, (1997), Application of neural networks to turbulence control for drag reduction. Physics of Fluids, **9**, (6), 1740-1747.

[8] C.H. Crawford and G.E. Karniadakis, (1997), Reynolds stress analysis of EMHD-controlled wall turbulence .1. Streamwise forcing. Physics of Fluids, **9**, (3), 788-806.

[9] T. Kato, Y. Fukunishi, and R. Kobayashi,(1997) , Artificial control of the three-dimensionalization process of T-S waves in boundary-layer transition. JSME International Journal Series B-Fluids and Thermal Engineering, **40**, (4), 536-541.

[10] S.N. Singh and P.R. Bandyopadhyay, (1997), Linear feedback control of boundary layer using electromagnetic microtiles. Journal of Fluids Engineering-Transactions of the ASME, **119**, (4), 852-858.

[11] P.A. Nelson, M.C.M. Wright, and J.L. Rioual,(1997), Automatic control of laminar boundary-layer transition. *AIAA Journal*, **35**, (1), 85-90.

[12] H.A. Carlson and J.L. Lumley, (1996), Active control in the turbulent wall layer of a minimal flow unit. Journal of Fluid Mechanics, **329**, 341-371.

[13] B.F. Farrell and P.J. Ioannou, (1996), Turbulence suppression by active control. Physics of Fluids, **8**, (5), 1257-1268.

[14] R.D. Joslin, G. Eriebacher, and M.V. Hussaini, (1996), Active control of instabilities in laminar boundary layers - overview and concept validation. Journal of Fluids Engineering-Transactions of the ASME, **118**, (3), 494-497.

[15] T. Lee, M. Fisher, and W.H. Schwarz, (1995), Investigation of the effects of a compliant surface on boundary-layer stability. Journal of Fluid Mechanics, Apr, **288**, 37-58.

[16] H. Choi, P. Moin, and J. Kim, (1994), Active turbulence control for drag reduction in wall-bounded flows. Journal of Fluid Mechanics, **262**, 75-110.

[17] P. Hackenberg, J.L. Rioual, O.R. Tutty, and P.A. Nelson, (1995), The automatic control of boundary-layer transition - experiments and computation. Applied Scientific Research, **54**, (4), 293-311.

[18] U. Rist and H. Fasel, (1995), Direct numerical simulation of controlled transition in a flat-plate boundary layer. Journal of Fluid Mechanics, **298**, 211-248.

[19] S. Hubbard and N. Riley, (1995), Boundary-layer control by heat and mass transfer. International Journal of Heat and Mass Transfer, **38**, (17), 3209-3217.

[20] R.D. Joslin, R.A. Nicolaides, G. Erlebacher, M.Y. Hussaini, and others, (1995), Active control of boundary-layer instabilities - use of sensors and spectral controller. *AIAA Journal*, **33**, (8), 1521-1523.

[21] V.J. Modi, S. Sthill, and T. Yokomizo, (1995), Drag reduction of trucks through boundary-layer control. Journal of Wind Engineering and Industrial Aerodynamics, **54**, 583-594.

[22] J. Jimenez, (1994), On the structure and control of near wall turbulence. Physics of Fluids, **6**, (2), 944-953.

[23] M.M. Elrefaee, (1994), Boundary layer control of separated flow over circular cylinders - a bem parametric study. Engineering Analysis with Boundary Elements, **14**, (3), 239-254.

[24] A.H.M. Kwong and A.P. Dowling, (1994), Active boundary-layer control in diffusers. *AIAA JOURNAL*, **32**, (12), 2409-2414.

[25] K. Zhou, J.C. Doyle and K. Glover, *Robust and optimal control*, (Prentice Hall, 1996).

[26] I. Rhee and J.L. Speyer, (1996), A game theoretic approach to a finite-time disturbance attenuation problem, IEEE Trans. Automatic Control, **36**, (9), 1021.

[27] S.S. Joshi, J.L. Speyer and J. Kim, (1997), A systems theory approach to the feedback stabilization of infinitesimal and finite-amplitude disturbances in plane Poiseuille flow, J. Fluid Mech., **332**, 157.

[28] S.S. Joshi, J.L. Speyer and J. Kim, Modelling and control of two dimensional Poiseuille flow, Proc. 34^{th} Conference on Decision and Control, New Orleans, Louisiana, December 1995, p. 921.

[29] H.H. Hu and H.H. Bau, (1994), Feedback control to delay or advance linear loss of stability in planar Poiseuille flow, Proc. Royal Soc. of London A, **447**, (1930), 299.

[30] L. Cortelezzi and J.L. Speyer, Robust reduced-order controller of laminar boundary layer transitions, submitted for publication to Phys. Rev. E

[31] K-H. Lee, Doctoral dissertation, in preparation.

[32] J.C. Doyle and G. Stein, (1981), Multivariable feedback design: Concepts for a classical/modern synthesis, IEEE Trans. Automatic and Control, **AC-26**, (2).

[33] M. Thak and J.L. Speyer, (1987), Modeling and parameter variations on asymptotic LQG synthesis, IEEE Trans. Automatic and Control, **AC-32**, (9).

[34] B.F. Farrell, (1988), Optimal excitation of perturbations in viscous shear flows, Phys. Fluids **31**, (8), 2093.

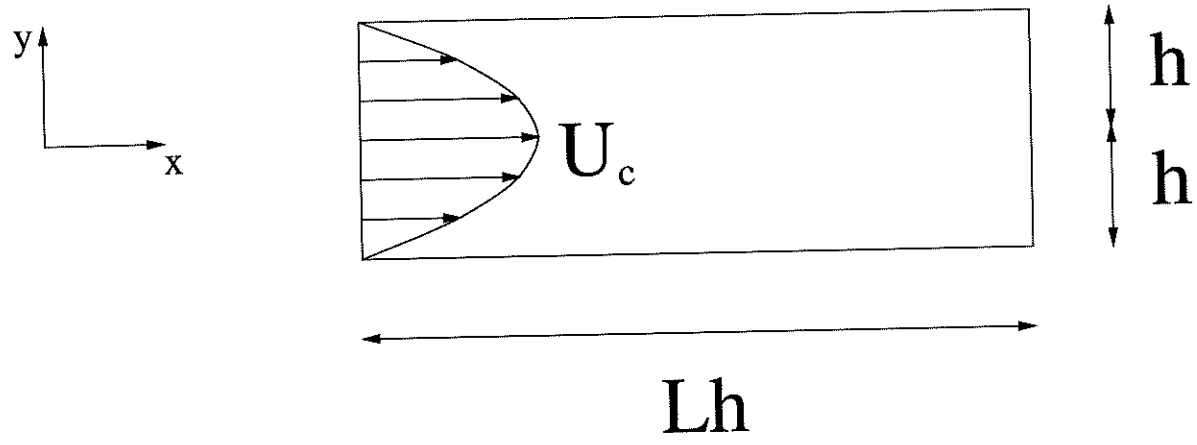

Figure 1: Flow geometry.

(a)

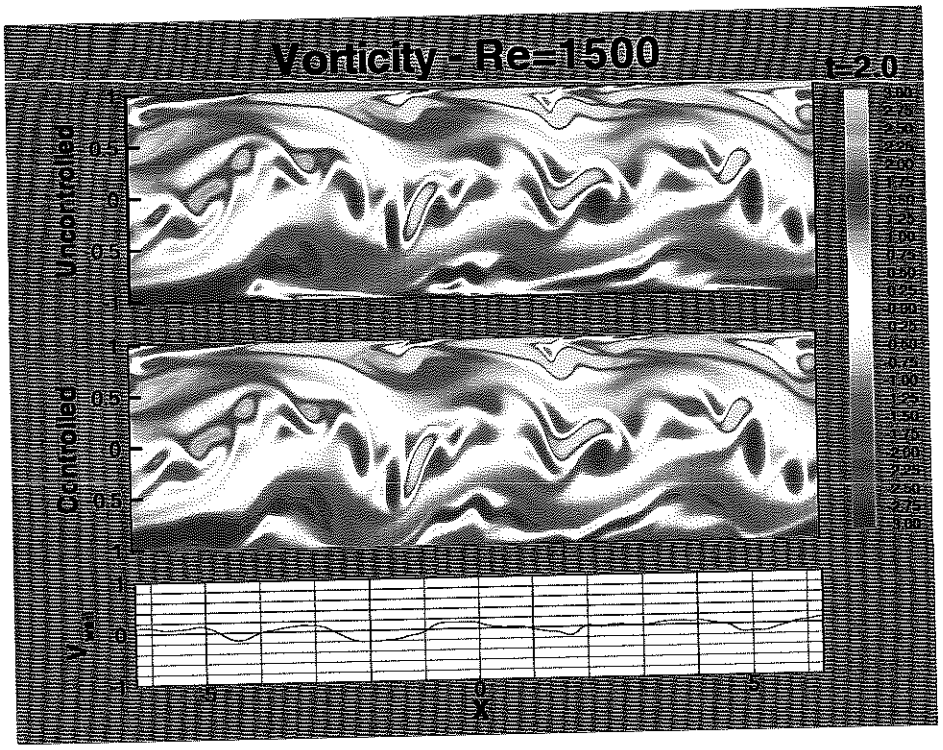

(b)

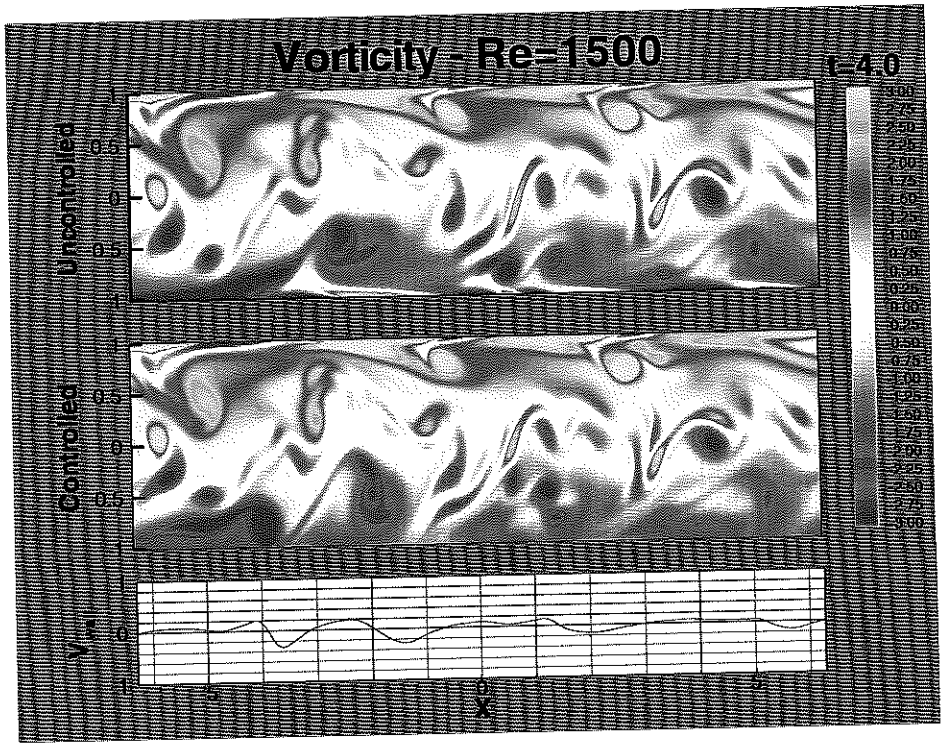

Figure 2: Vorticity field for the uncontrolled and controlled case amplitude of v_w at time t=2 (a), 4 (b).

(a)

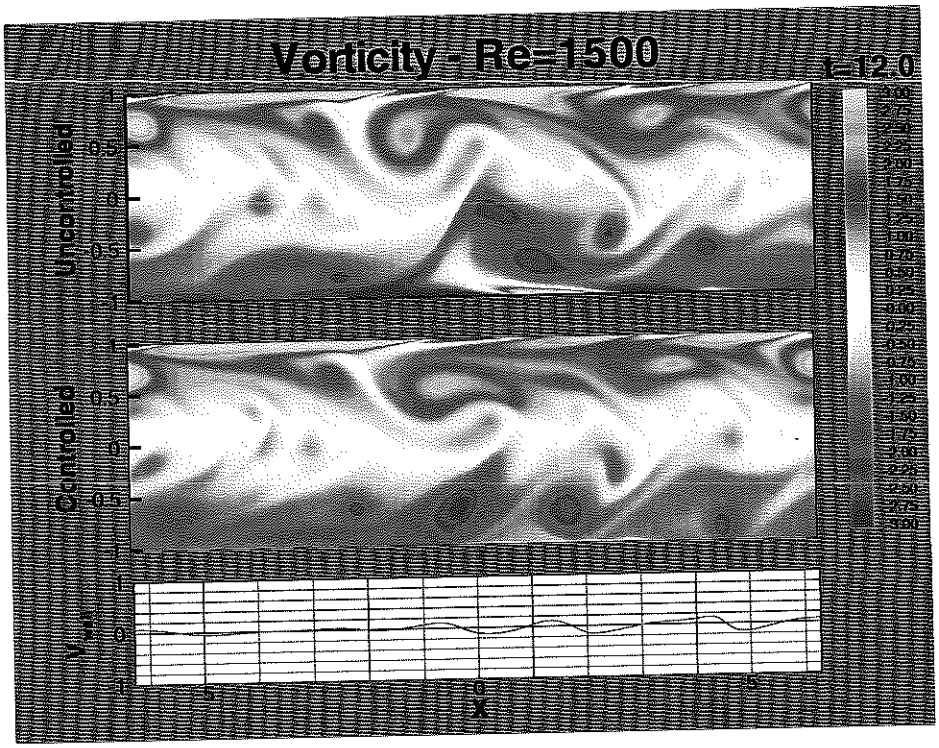

(b)

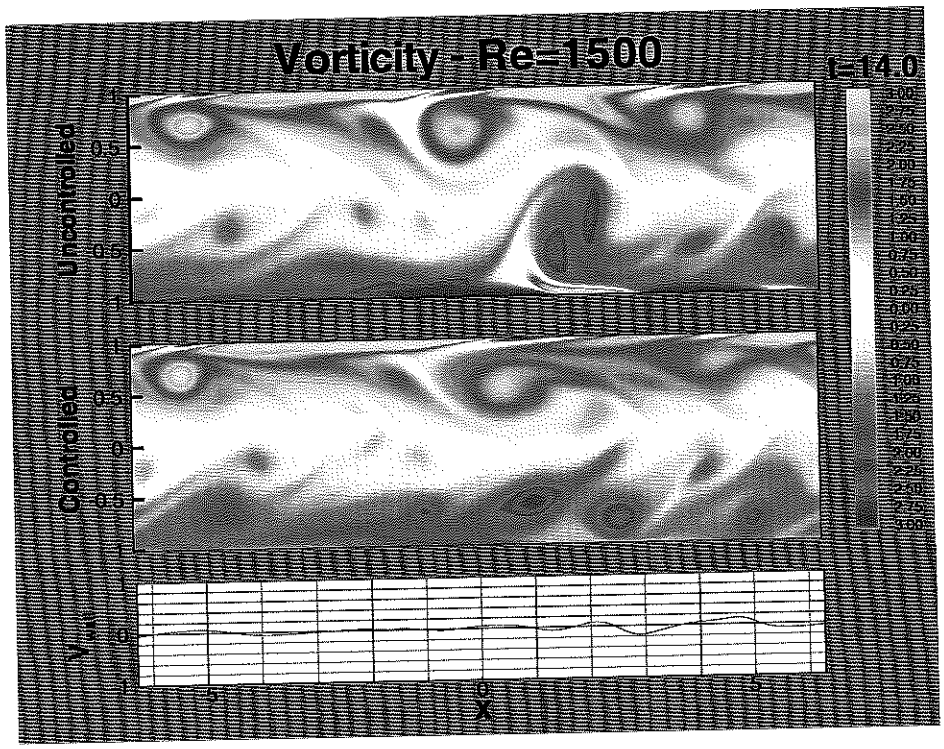

Figure 3: Vorticity field for the uncontrolled and controlled case amplitude of v_w at time t=12 (a), 14 (b).

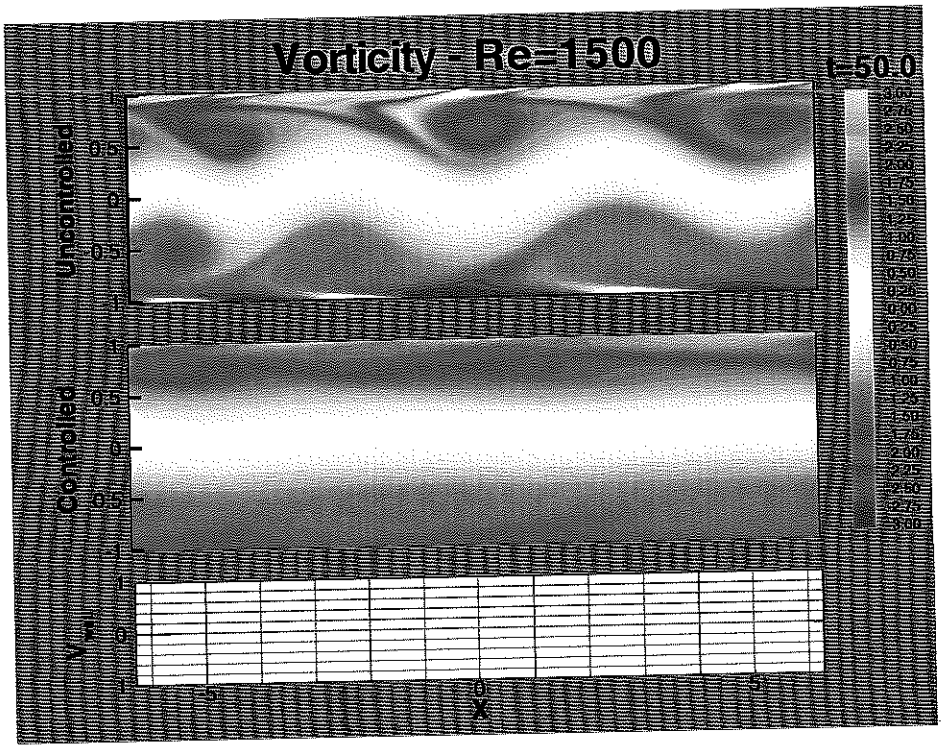

Figure 4: Vorticity field for the uncontrolled and controlled case amplitude of v_w at time t=50.

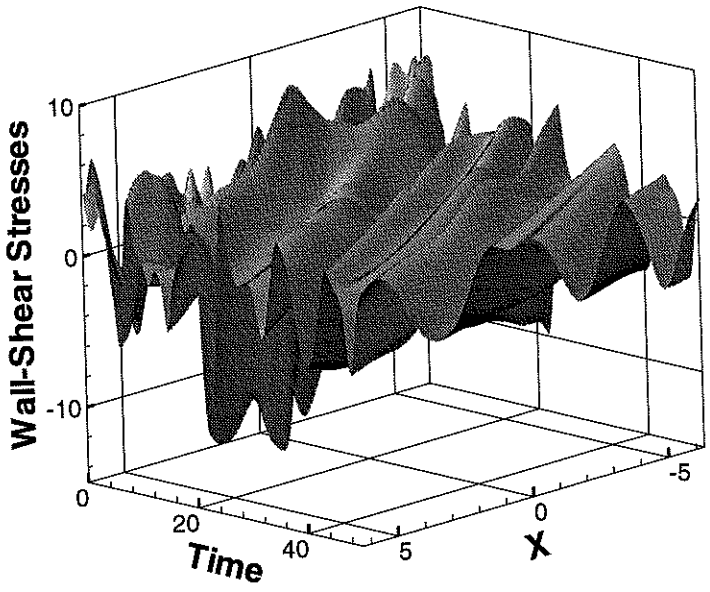

Figure 5: Time evolution of the wall-shear stresses along the bottom wall of the channel in the uncontrolled case.

(a)

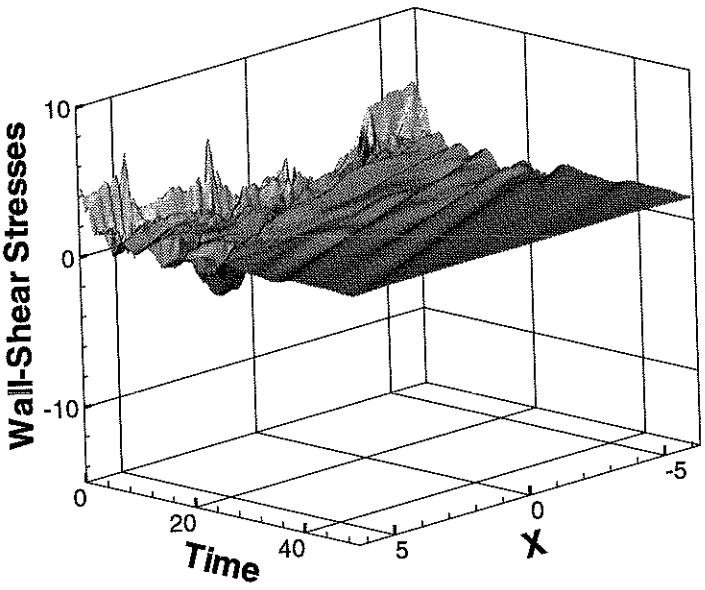

(b)

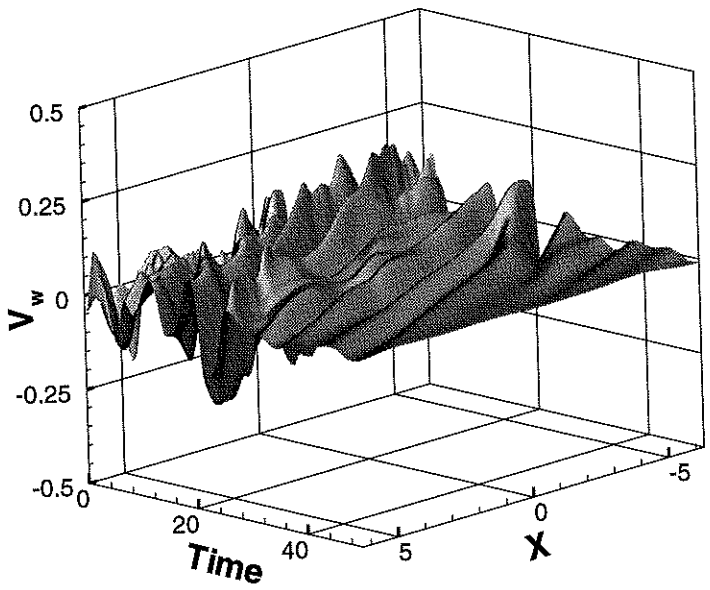

Figure 6: Time evolution of the wall-shear stresses (a) and blowing and suction (b) along the bottom wall of the channel with all the controllers operating.

(a)

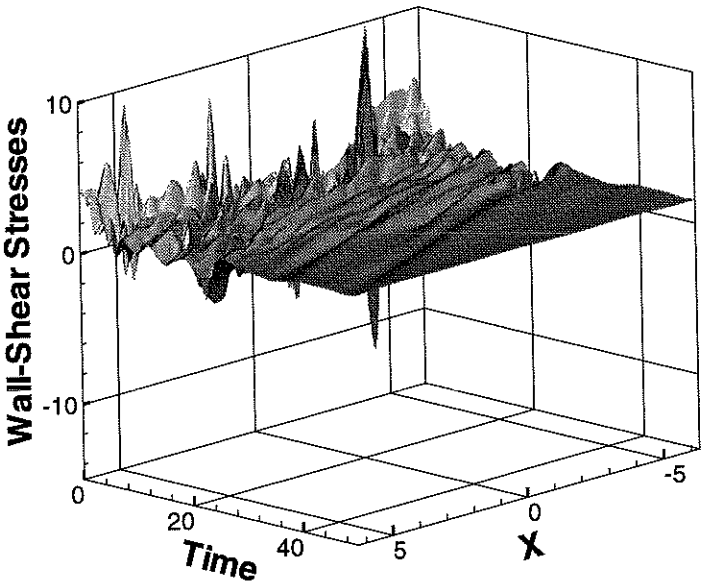

(b)

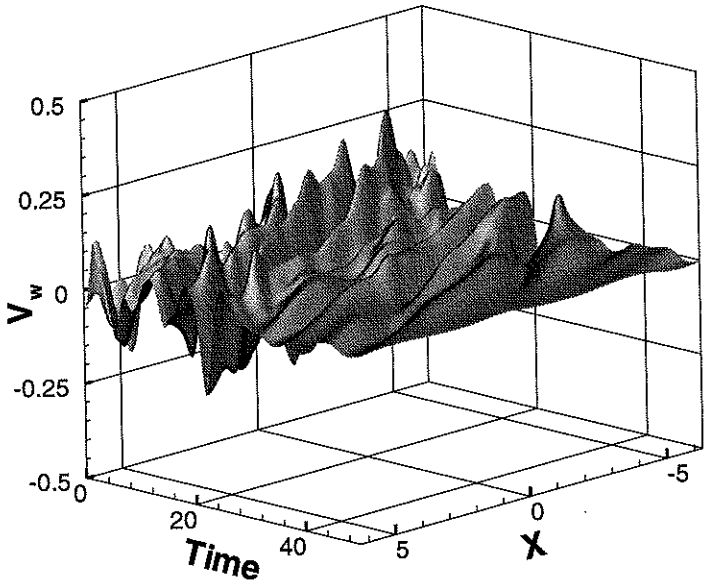

Figure 7: Time evolution of the wall-shear stresses (a) and blowing and suction (b) along the bottom wall of the channel with all the controllers operating only on wave numbers 1 through 16.

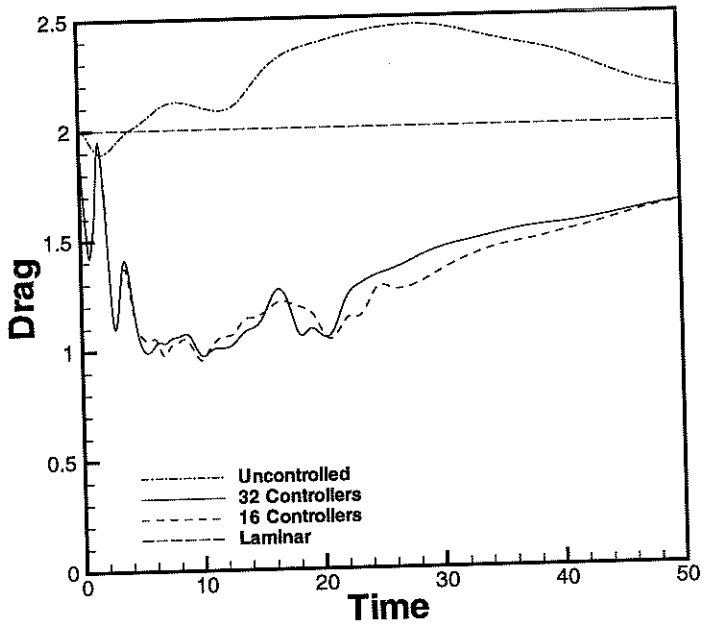

Figure 8: Comparison of the total drag measured at the bottom wall of the channel: laminar flow, uncontrolled turbulent flow, fully and partially controlled turbulent flow.